The Ionized Gas Kinematics of the LMC-type galaxy NGC 1427A in the Fornax Cluster[1]

J. Chanamé, L. Infante, and A. Reisenegger

Departamento de Astronomía y Astrofísica, Pontificia Universidad Católica de Chile, Casilla 306, Santiago 22, CHILE

Received ______________________; accepted ______________________

[1]Based on data collected at Las Campanas Observatory, Chile, run by the Carnegie Institution of Washington

ABSTRACT

NGC 1427A is a LMC-like irregular galaxy in the Fornax cluster with an extended pattern of strong star formation around one of its edges, which is probably due to some kind of interaction with the cluster environment. We present Hα velocities within NGC 1427A, obtained through long-slit spectroscopy at seven different positions, chosen to fall on the brightest H II regions of the galaxy. Due to its location very near the center of the cluster this object is an excellent candidate to study the effects that the cluster environment has on gas-rich galaxies embedded in it. The rotation of NGC 1427A is modeled in two different ways. The global ionized gas kinematics is reasonably well described by solid-body rotation, although on small scales it shows a chaotic behaviour. In this simple model, the collision with a smaller member of the cluster as being responsible for the peculiar morphology of NGC 1427A is very unlikely, since the only candidate intruder falls smoothly into the general velocity pattern of the main galaxy. In a more elaborate model, for which we obtain a better solution, this object does not lie in the same plane of NGC 1427A, in which case we identify it as a satellite bound to the galaxy. These results are discussed in the context of a normal irregular versus one interacting with some external agent. Based on several arguments and quantitative estimates, we argue that the passage through the hot intracluster gas of the Fornax cluster is a very likely scenario to explain the morphological properties of NGC 1427A, although our kinematical data are not enough to support it more firmly nor rule out the possibility of a normal irregular.

Subject headings: galaxies: cluster: individual (Fornax) — galaxies: interactions — intergalactic medium — ISM: kinematics and dynamics — shock waves

1. Introduction

Interactions between galaxies and their environments are thought to be important mechanisms driving galaxy evolution. For example, they have been invoked to explain the excess of blue galaxies in high redshift clusters relative to present-day clusters, the so-called Butcher-Oemler effect (Butcher & Oemler 1978; Gunn 1989; Evrard 1991). Clusters of galaxies are ideal places to study these interactions, due to their great concentration of galaxies of various morphologies, sizes and luminosities, and huge masses of gas, in a comparatively small volume of space. Among the various kinds of interactions that could be experienced by a cluster galaxy we have: tidal forces from another galaxy or from the cluster as a whole (Byrd & Valtonen 1990; Henriksen & Byrd 1996), the ram pressure from the passage through the intracluster medium (ICM) (Gunn & Gott 1972; Giovanell & Haynes 1985; Evrard 1991; Phookun & Mundy 1995), high-speed encounters between galaxies (Moore et al. 1996), collisions and mergers (Lynds & Toomre 1976; Theys & Spiegel 1977; Barnes & Hernquist 1991), and the combined action of two or more of these mechanisms (Patterson & Thuan 1992; Lee, Kim, & Geisler 1997).

The Fornax cluster is a relatively poor galaxy cluster dominated by early-type galaxies. Compared to Virgo, the center of Fornax is two times denser in number of galaxies, but Virgo as a whole is almost four times richer (Ferguson & Sandage 1988; Hilker 1998). The hot ICM of Fornax shines in X-rays, as detected by ROSAT and ASCA (Jones et al. 1997; Rangarajan et al. 1995; Ikebe et al. 1996), and this hot gas extends at least 200 kpc from the center of the cluster. Two giant ellipticals, NGC 1399 (a cD galaxy with an extended halo of about 400 kpc in diameter, and an extraordinarily large population of globular clusters, see Hilker 1998; Grillmair et al. 1999) and NGC 1404, lie at the center of the cluster. Fornax may be composed of two subclusters in the process of merging, evidenced by the big relative radial velocity between NGC 1399 and NGC 1404 of about

500 km/s (Bureau, Mould, & Staveley-Smith 1996). However, these galaxies are close in space. Distance determinations based on surface brightness fluctuations (Jensen, Tonry, & Luppino 1998) and globular cluster luminosity functions (Richtler et al. 1992; Grillmair et al. 1999) put them at roughly the same distance. Moreover, the X-ray observations with ROSAT show that the hot corona associated with NGC 1404 is distorted and probably being stripped, indicating an infall of this galaxy towards NGC 1399 and the cluster center (Jones et al. 1997).

NGC 1427A is the brightest irregular (Irr) galaxy in the Fornax cluster, and very similar to the LMC in its morphology and colors (Hilker et al. 1997). The great majority of the high surface brightness regions that dominate the light of NGC 1427A are aligned along the south-western edge of the galaxy, in a kind of distorted ring (see Fig.1 and Fig.5). Several arguments point towards explaining the appearance of this galaxy in the context of an interaction with its environment. The resemblance to the so-called ring galaxies led Cellone and Forte (1997) to suggest that NGC 1427A is the result of an encounter with a smaller intruder, giving also a candidate for this intruder (the North Object, see Fig. 1 and Fig. 5). NGC 1427A is also very close to the center of the cluster, with a projected distance of 121 kpc to NGC 1399 and 83 kpc to NGC 1404 [2], so tidal forces might be important in the enhancement of the star formation in the galaxy. Finally, NGC 1427A is crossing the ICM of Fornax at a supersonic speed (see Section 4), so the ram pressure exerted by the intracluster gas could also be the cause of the peculiar distribution of star forming regions in the galaxy. Gavazzi et al. (1995) studied three galaxies in the cluster Abell 1367 which, like NGC 1427A, have their bright H II regions distributed along one edge of their perimeters,

---

[2]Throughout this paper we assume a distance to the Fornax cluster of 18.2 Mpc, from Kohle et al. (1996), recalibrated as in Della Valle et al. (1998) using the new distances to Galactic globular clusters from Hipparcos (Gratton et al. 1997).

which they attribute to the increase of the external pressure as the galaxies cross the ICM.

In this paper we present the kinematics of the ionized gas (H II regions) of NGC 1427A and discuss the obtained velocity field in the context of a normal Irr galaxy versus an interacting galaxy. In Section 2 we describe the observations, reduction of the data and the error analysis. In Section 3 we model the kinematics of the galaxy and analize the results. Section 4 contains the discussion of the possible scenarios for the history of NGC 1427A in the light of our results, and in Section 5 we give our conclusions.

2. Observations, Data Reduction and Error Analysis

Long-slit spectra of NGC 1427A were obtained during two runs with the 2.5m DuPont telescope at Las Campanas Observatory, Chile, during 1997 February 3-4 and August 9-14. The telescope was equipped with the Modular Spectrograph. The grating used had 600 grooves/mm, and as the detector we used a 2048×2048 SITe chip, with a pixel size of 15 μm. This setup gives a dispersion of 1.27 $\AA$/pix and a spatial sampling of 0.3625 arcsec/pix. On the February run the measured seeing was about 1 arcsec during the entire night, which corresponds to a linear scale of 88 parsec at the adopted distance to Fornax. For the August run, due to the presence of some clouds, we binned the spatial direction by a factor of 2 in order to get more light, obtaining 0.725 arcsec/pix. The seeing was 1.4 arcsec, resulting in a spatial resolution of 123 parsec. Integration times were of 45 minutes at the slit positions where three 15-minute frames were obtained, and 15 minutes otherwise. The instrumental resolution was derived by measuring the FWHM of several unblended lamp lines after calibrations. For the February run we obtained a mean FWHM of 2.98 $\AA$, corresponding to a standard deviation of the Gaussian $\sigma = 1.27$ $\AA$ (i.e., 58 km/s at Hα), and a mean FWHM of 4.8 $\AA$ for the August run, corresponding to $\sigma = 2.05$ $\AA$ (i.e., 93 km/s at Hα). The wavelength range is 4700 $\AA$ - 6850 $\AA$ for the February run and 4800 $\AA$

- 6960 $\AA$ for the August run. This range includes several emission lines of the ionized gas, namely, Hβ, [OIII], HeI, [NII], Hα, and [SII] (see Fig. 2). The slit was aligned in order to cover the majority of the bright H II regions of the galaxy. The positions of the slits are shown in Fig. 1 and were derived by matching coordinate information obtained on the guider screen during the observations with an Hα image of the galaxy. The coincidence between the spatial profiles along the slits and their inferred positions on the galaxy was almost perfect. The images show the strong emission lines of the H II regions, but very weak emission coming from the regions between them, so we are mostly restricted to work with the brightest regions of recent star formation. In the majority of the cases three frames were obtained on each position in order to deal with cosmic rays.

EDITOR: PLACE FIGURE 1 HERE.

EDITOR: PLACE FIGURE 2 HERE.

The data reduction was done using the IRAF[3] software package. All the images were bias subtracted, flat-fielded using normalized continuum lamps, and then the frames for each slit position were combined to produce the final images. Because some of the H II regions we observed are very faint, the extraction of their spectra was done with great care. First, we extracted the spectrum of a standard star with a very strong flux and used this image as a reference for the tracing of the spectra of the fainter H II regions. Finally, for the background subtraction we used samples of sky as close as possible to the H II regions, fitting the level of this background (night sky plus the background light of NGC 1427A) with a low-order polynomial.

---

[3]IRAF is distributed by NOAO, which is operated by the Association of Universities for Research in Astronomy Inc., under contract with the National Science Foundation.

The wavelength calibration was done using He-Ne lamps taken just before or just after each exposure. We identified 23 good lines, with which we constructed dispersion solutions with a fifth-order Legendre polynomial, always obtaining a residual RMS of less than 0.1 $\AA$. To measure the radial velocities we first fitted the continuum and then subtracted it from every spectrum, so we are finally left with just the emission lines. By far the strongest line in all our spectra is Hα. This, along with the fact that there were far more comparison lines, evenly distributed, on the red side than the blue side of the wavelength range, making the dispersion solution better on the red side, led us to use just the Hα emission to measure the velocities. Once the continuum was subtracted, the velocities were measured by fitting a Gaussian profile to the line to obtain the center, and with this center we obtained the radial velocity by using the standard Doppler formula. Finally we applied the heliocentric correction to all the Hα velocities.

EDITOR: PLACE TABLE 1 HERE.

To estimate the errors in our velocities we extracted various sky spectra from each of the final images, selected ten to twelve night emission lines at various signal-to-noise ratios (defined as S/N $= f/(f + n(ron)^2 + n(sky))^{1/2}$, where f is the flux in electrons contained in the emission line after the continuum was subtracted, *sky* is the continuum level at the emission line in electrons per pixel, n is the width of the line at zero intensity in pixels, and *ron* is the readout noise in electrons/ADU), and measured the centers of all these lines following the same procedure as for the Hα velocities. Then we plotted the difference between each measurement and the average of all the measurements of the same line (which we call the residual) versus S/N. In total we had approximately 1300 data points, which we grouped in bins and plotted. The results are shown in Fig. 3a. To assign the error to a velocity, we measure the S/N of the corresponding Hα line and interpolate using the diagonal rational function (Press et al. 1992) at that S/N. The data are given in Table 1,

where the coordinates refer to the axes shown in Fig. 1 and Fig. 5, and the origin is not included in the images.

EDITOR: PLACE FIGURE 3 HERE.

We performed another method of error estimation by means of a Monte Carlo simulation. We constructed an artificial spectrum consisting of one perfectly gaussian emission line (i.e., we exactly know its center, width and amplitude) placed in the wavelength region where we observe the Hα line in our spectra. Then, using IRAF routines, Poisson noise was added randomly to the 'perfect' spectrum (using the same gain, 0.8 electrons/ADU, and read-out noise, 3 electrons, as the chip used during the observations), creating one thousand 'noisy' spectra. Next, we added to these artificial spectra real sky randomly extracted from the regions of NGC 1427A where no H II regions are present. Finally, we applied to these semi-artificial spectra the same measuring process as for the Hα velocities. A histogram of all the measurements fits well with a Gaussian curve (which tells us that the measurement errors are normally distributed, an important point when discussing modeling of the velocity field, see Section 3), whose standard deviation we took as the error estimated for a representative S/N of all the artificial spectra. We automatized this whole procedure and repeated it for many different S/N ratios, obtaining results quite similar to those obtained with the analysis of the skylines. We chose then to adopt the night skylines method as our error estimation.

3. Kinematic models.

In Fig. 4 we show the measured Hα heliocentric velocities of the 29 positions over the galaxy for which we measured reliable data. The velocities are plotted as a function of the distance to the axis of rotation, whose position was obtained as we will explain later

in this section. On local scales, the data show a state of complex kinematics, with very close points whose velocities do not overlap within their error bars. It is not uncommon for these clumpy Irr galaxies to show disordered patterns in their velocity fields (e.g. Hunter & Gallagher 1986), but the large scatter of velocities observed in NGC 1427A and the particular characteristics of its environment make us suspicious about treating it as a normal Irr. On a global scale, one can see that there is a rotation present, with an amplitude of about 150 km/s from one side of the galaxy to the other. Most Irr galaxies, unlike spirals (which usually show amplitudes in the rotation speeds of 400 km/s from end to end), are slow rotators, showing near rigid-body behaviour extending over most of their optical dimensions (e.g. Gallagher & Hunter 1984; Hunter & Gallagher 1986). In NGC 1427A it is clear that the velocity rises from east to west following a roughly linear trend (corresponding to solid-body rotation), *but with a large scatter between the data points and the fitted line* (see Fig.4). It is clear that any smooth, conventional model of rotation curve will not be capable to follow such a large scatter. However, trying to adjust some simple models to the data will uncover overall characteristics and give some insights about the nature of the velocity field of the galaxy.

EDITOR: PLACE FIGURE 4 HERE.

As a first approximation, we tried to fit a rigid-body rotation model,

$$v_{l.o.s.} = v_0 + (\omega \times \mathbf{r}) \cdot (-\mathbf{z}) = \mathrm{v_0} + \omega_{\mathrm{y}}\mathrm{x} - \omega_{\mathrm{x}}\mathrm{y},$$

where v_0 is the recession velocity of the (arbitrary) origin of the x-y coordinates on the plane of the sky (see Table 1), $(-\mathbf{z})$ is a unit vector along the line of sight, and ω_x and ω_y are the components of the angular velocity vector ω projected on the plane of the sky (X being the E-W direction and Y the N-S one, see Fig. 4). This model does not yield any information concerning the center of rotation nor an inclination of the disk of the galaxy. A linear

least-squares fit gives a best-fit model with χ^2=134, and a reduced χ^2, or χ^2 per degree of freedom, of $\chi^2/(N-M)$=5.2, where N=29 is the number of data points, and M=3 the number of parameters to adjust. This is a large value for the merit function that is not acceptable in order to adopt the model as a good one. However, the results are still valid as a first approximation to the magnitude and direction of the rotation. The best-fit model parameters obtained were 1.29±0.05 and -12.8±0.1 km/s/kpc for ω_x and ω_y respectively, and one can see that, as expected from simple inspection, the rotation projected on the sky is almost entirely around the N-S axis. These values for the components of the angular velocity vector imply an axis of rotation on the plane of the sky whose direction is inclined 6° counter-clockwise from the vertical direction. The shallow velocity gradient of about 13 km/s/kpc is in agreement with what is observed in most Irrs, having ≈ 5-20 km/s/kpc (Gallagher & Hunter 1984).

Next, we used a model after de Zeeuw and Lynden-Bell (1988), which assumes that the gas lies in a flat disk following circular orbits. The model represents a family of rotation curves, parametrized by

$$v_{rot}(r') = \frac{Vr'}{(r'^2 + r_0^2)^{p/2}}.$$

Here, V, r_0, and p are constant parameters, and r' is the distance from each point to the center of rotation measured on the plane of the galaxy. Note that the solid-body (p=0), flat (p=1), Keplerian (p=3/2), and other models of rotation curves are special cases of this family. To allow for an arbitrary inclination of the disk of the galaxy with respect to the sky, we did the following. First, using the center of rotation (x_0, y_0) as origin of coordinates, we rotated the X and Y axes (i.e., the plane of the sky) by an angle β around the line of sight Z, obtaining the system $X''Y''Z''$, with $Z'' = Z$. After the fitting, this angle will tell us about the direction of the axis of rotation projected onto the sky. Then we made a second rotation, now around the X'' axis, tilting the $X''Y''$ plane by an angle α, obtaining

the system $X'Y'Z'$. The disk lies in the $X'Y'$ plane, and the Z' axis is parallel to the angular momentum vector of the rotating disk. The angle α, then, sets the inclination of the galaxy with respect to the plane of the sky. In order to fit this model to our data, we project the velocity of rotation along the line of sight (the $-Z$ direction), so the equation to fit is

$$v_{l.o.s.} = v_0 + v_{rot}(r') \sin\alpha \cos\theta'.$$

Here v_0 is the systemic velocity of the galaxy, and θ' is the angle between the position vector $\mathbf{r}'$ and the X' axis. This equation depends on eight parameters $(v_0, \beta, \alpha, V, x_0, y_0, r_0, p)$, the majority of them in a nonlinear way. We developed a code that, using the Levenberg-Marquardt method of nonlinear fitting (Press et al. 1992), returns the values for the parameters that minimize the χ^2 merit function.

EDITOR: PLACE FIGURE 5 HERE.

In terms of the final value of χ^2, the best-fit de Zeeuw & Lynden-Bell model resulted closer to the data than the pure rigid-body rotation, but it is still not a good fit. A careful inspection of each step during the process of iteration to the best-fit model shows that the parameters v_0, β, α, x_0, and y_0, quickly converge to their final, best-fit values. The best-fit value for the systemic velocity v_0 is 2039 km/s, in reasonable agreement with the H I systemic velocity measured by Bureau et al. (1996). The best-fit center of rotation, shown as a cross in Fig. 5, is located approximately 12 arcsec to the west of the midpoint between the optical edges of the galaxy. We obtained an angle $\beta = 10°$, counter-clockwise from the N-S direction (see Fig. 5), close to the inclination found using the solid-body model. For the inclination of the disk with respect to the sky, α, the best-fit value was 80°, which would correspond to a disk seen almost edge-on (see Section 4 for the implications of this

high inclination). However unexpected, this value of α is reached quickly by the algorithm. It does not agree with the inclination reported by Bureau et al. (1996) of $\alpha = 48°$, derived using the photometric axial ratio, a rather arbitrary criterion for a galaxy like NGC 1427A. Having arrived at this point of the fitting procedure, the merit function reaches a flat valley in parameter space, with $\chi^2 \approx 80$, and χ^2 per degree of freedom of ≈ 3.8[4]. The parameters p, V, and r_0 are degenerate, in the sense that there is no unique set that gives a global minimum of χ^2. It is clear from the expression for v_{rot} that, as p increases, V also has to rise in order to keep v_{rot} constant. This is indeed what the fitting algorithm shows. Setting $p = 1$, we find $V = -75$ (in km/s only for this value of p, and the sign indicating the direction of the spin), r_0=2.7 kpc, and χ^2=83. For $p = 1.2$, $V = -220$, and $r_0 = 2.9$ kpc, we have $\chi^2 = 81$. And finally, for $p = 1.5$, $V = -1175$, and $r_0 = 3.7$ kpc, the χ^2=79, almost negligibly better than the model with $p = 1$. For values of p <1 the obtained χ^2's begin to rise quickly. As one can see, it is not possible to distinguish between models with $1 \leq p \leq 3/2$, because the data are scarce at distances from the center where the models begin to differ from each other. This is shown in Fig. 6, where the data have been projected onto the plane of the disk (dividing the corresponding velocities by $\sin\alpha\cos\theta'$), and the corresponding error bars rescaled (note that we didn't take the error in the scaling factor into account). Data points marked as triangles lie very close to the axis of rotation, making the factor $\cos\theta'$ very small and uncertain in its sign. This is reflected by meaningless values of v_{rot}, possibly with the wrong sign, as well as very large (but still underestimated) error bars.

EDITOR: PLACE FIGURE 6 HERE.

---

[4]For comparison, if we fix the value of $\alpha = 48°$ and run the fitting program, we obtain a minimum χ^2=122.

We explored the possibility that the models fail to explain the data due to problems with our error estimation. Of course, if we multiply the errors in the measured velocities by a factor of, say, 1.5, then the resulting value of χ^2 would be acceptable. But we are quite confident that our quoted errors are not underestimated, having obtained them by means of two different methods, one of them based on the actual set of data. Also, one could obtain a bad fit, even with the correct model, if the quoted errors were not normally (Gaussian) distributed. The reason for this is that the minimization of the merit function χ^2 *assumes* that the errors are normally distributed (Press et al. 1992). We tested this possibility by building (for both methods of error estimation) the distribution of the errors and fitting a Gaussian function to them. In both cases the agreement was very good, as seen in Fig. 3b for the method using skylines, so we reject this possibility. All the previous attempts to fit a model to the data and the above discussion about the distribution of the errors was regarding the estimated errors in the velocities. So far we have assumed that we know *exactly* the positions (x, y) of the regions whose spectra we have. So, in order to quantify the changes in the fitting results when some uncertainty in the coordinates is introduced, we performed the following exercise. We took the coordinates (x, y) of all the data points and changed randomly their values around the original ones, after which we adjusted the rigid-body model to the "new" data set. We estimate a "real" uncertainty in the coordinates to be no more than 2 arcsec in the worst of the cases, so the changes introduced in the coordinates were randomly distributed between plus or minus 2 arcsec. Repeating the procedure two or three thousand times, always in a random way, we found that ω_x, ω_y, and χ^2 never change by a large amount. Doubling the uncertainty to 4 arcsec does not make any difference, so we conclude that there is no need to worry about uncertainties in the coordinates. Finally, since we are interested in relative velocities, eventual systematic errors should not affect our results as long as they affect all velocities in the same way.

4. Discussion

4.1. Kinematics

We have presented the velocities of the ionized gas from many of the brightest H II regions in NGC 1427A, and modeled them to derive the basic properties of its dynamics. Using two different models for the kinematics we found the major axis of rotation, with both solutions in reasonable agreement.

The simplest model, a global rigid-body rotation plus a random component on small scales (responsible for the poor fit), seems to be a good approximation to the data (Fig. 4), and is in concordance with what is observed in most Irr's. The radial velocities of points in the North Object match well with this model (see Fig. 4), which suggests that it is part of the galaxy, as the rest of the H II regions. However, if we want information about the center of rotation and the inclination of the galaxy, we need a more elaborate model. Our solution using the de Zeeuw & Lynden-Bell model is better than the solid-body one in terms of the merit function χ^2 but, here again, the random component dominates the appearance of the rotation curve (Fig. 6). The puzzling feature of this solution is the remarkably high inclination (80°) returned by the fit, which does not depend on whether we use the points in the North Object in the fitting procedure. Assuming that the North Object is part of NGC 1427A and that it lies in the same disk as the rest of the H II regions, this inclination would place it at a distance of about 30 kpc from the fitted (and optical) center of NGC 1427A, which is difficult to believe. If we lower the angle of inclination until the one derived using the photometric axial ratio (Bureau et al. 1996) this problem is softened, with the North Object at 8.2 kpc, but with a χ^2 50% higher than before. So, we are inclined to place the North Object outside the disk of NGC 1427A. We estimated the probability of the chance coincidence that the North Object being an independent cluster member with its velocity in the same range as those of the H II regions of NGC 1427A (1950-2100 km/s). Assuming

for the cluster galaxies a Gaussian radial velocity distribution (which is the case when the three dimensional distribution is Maxwellian) centered at NGC 1399 (1430 km/s) and with a dispersion of 325 km/s (Bureau et al. 1996), we obtain a probability of 3.5% of a chance coincidence. This low probability, the North Object lying outside the plane of the galaxy, and the coincidence in the radial velocities would indicate that it is a separate object but gravitationally bound to NGC 1427A, probably a small satellite orbiting the galaxy.

Based on the previous results, we estimated the dynamical mass and other related quantities for NGC 1427A. Taking the angular velocity obtained from the solid-body fit and assuming a spherical mass distribution, the total mass inside a radius of 6.2 kpc (the size of the major axis at the 24.7 mag/arcsec^2 isophote in V) is $M_{dyn} \gtrsim (9 \pm 3)\text{x}10^9 M_\odot$ [5]. This is a lower limit for the total mass inside this radius because of the unknown component of the angular velocity along the line of sight. However, if the inclination of the disk is really as high as 80°, then this unknown component will not be very relevant, and the quoted value for M_{dyn} will be close to the actual one. The mass in the form of neutral hydrogen can be obtained from the integrated H I flux (Bureau et al. 1996) and the adopted distance to Fornax, using the formula of Roberts (1975). With this, the H I mass turns out to be $M_{H\,\textsc{i}}$ $= (1.8 \pm 0.3)\text{x}10^9 M_\odot$, so the fraction of the total mass in the form of neutral hydrogen is approximately 0.2, twice the value for the LMC (based on the total mass from Kunkel et al. 1997 and the H I flux from Huchtmeier & Richter 1988). Finally, from the magnitudes given by Hilker et al. (1997), the mass-to-light ratios for NGC 1427A are $M/L_B \gtrsim 3.9$, and $M/L_V \gtrsim 4.8$, in units of solar masses per solar luminosities in the corresponding band. As a comparison, the LMC has a mass-to-light ratio of $\approx 2.9 M_\odot/L_\odot$ in the B band (from the

[5]The uncertainty in the total mass is almost entirely due to the uncertainty in the size of NGC 1427A, which is a combination of uncertainties in the angular size of the galaxy and the distance to Fornax.

magnitudes given by de Vaucouleurs et al. 1991 and the total mass of Kunkel et al. 1997). The values obtained for the total mass of NGC 1427A, the fraction of H I in it, as well as the mass-to-light ratio, all are in good agreement with typical values for the latest galaxy types, as summarized by Roberts & Haynes (1994).

The random behaviour on small scales is not difficult to understand. Since the aperture sizes of our spectra vary between 4 and 12 arcsec, corresponding to spatial extensions in the range 0.3 - 1 kpc on the galaxy, our velocities are actually averages taken over structures and regions of various sizes. On these scales it is very common to find in these galaxies structures such as shells and supershells, large-scale filaments of ionized gas, as well as a non-negligible component of diffuse ionized gas (Hunter & Gallagher 1986; Martin 1997, 1998). All these structures reflect the strong impact that massive stars have on their surroundings, injecting large amounts of energy via stellar winds and supernova shocks. Hints of two supershells can be seen in the optical images of NGC 1427A, with diameters of 0.7 and 1.1 kpc (see Fig. 7), apparently emerging from the largest of the high surface brightness features. These structures seem to be primarily photoionized, despite their location very far from the nearest star associations (Hunter & Gallagher 1997; Martin 1998), and show expansion velocities between 20 and 60 km/s, sometimes going up to 100 km/s (see Fig. 3 in Martin 1998). The filled circles in the rotation curve of Fig. 4 correspond to the brightest H II regions seen in Fig. 5, and one can see that they are closer to the solid-body line than the blank circles, which correspond to diffuse ionized gas some distance away from the bright H II regions. This diffuse gas should be more subject to the effects of expanding shells and filaments, and this could be the reason why they depart from the overall rotation. The largest discrepancies in our data are between 40 and 70 km/s, so it is very likely that some of them are due to the strong influence of very massive stars on the ISM. Furthermore, part of the diffuse gas may not be in the disk of the galaxy, but instead it could have been transported into the halo by some mechanism (see, e.g., Dahlem,

Dettmar, & Hummel (1994) for ionized gas away from the disk in NGC 891, and also Bomans, Chu, & Hopp (1997) for gas outflows from intense star forming regions in NGC 4449), where it would not necessarily corotate with the disk. Nevertheless, considering only the bright H II regions does not improve the fits (the dispersion is smaller, but so are the error bars). Therefore, some physical mechanism (winds, turbulence, ...) must still be involved to explain the $\approx$ 10-15 km/s discrepancies.

EDITOR: PLACE FIGURE 7 HERE.

4.2. Interaction with the cluster environment

Hilker et al (1997) and Cellone & Forte (1997) already suggested, based on morphological reasons and colours of the H II regions, that the appearance of NGC 1427A is due to an interaction with the Fornax Cluster environment. This possibility is very likely given the location of NGC 1427A near the center of the cluster. Based on the obvious alignment of the bright giant H II regions along a half ring at the south western part of the galaxy and the colors of the only two bright knots at the extreme north ("the North Object"), Cellone & Forte suggested that this could be the encounter between two different objects, the North Object being one of the many dwarf ellipticals that populate the center of the Fornax Cluster. As we said before, assuming a solid-body rotation, the velocities for the North Object fall well into the general kinematical pattern, which would indicate, with high probability, that it is just another part of NGC 1427A, not an intruder galaxy. On the other hand, if we take the de Zeeuw & Lynden-Bell model as the valid one, then we would have to accept that the North Object is not in the same disk as the rest of the H II regions, possibly being a satellite galaxy of NGC 1427A. The proximity of the two giant ellipticals of the cluster, NGC 1399 and NGC 1404, suggests that NGC 1427A might

be experiencing strong tidal forces. Tidal interaction is also a proposed mechanism for triggering star formation, but it seems unlikely that this could produce the ring-like pattern of star forming regions along one edge of the galaxy. Tides are known to produce thin low surface brightness filaments that stretch out from interacting galaxies (Gregg & West 1998). A search for tails at this low surface brightness would be possible with the use of wide-field imaging plus relatively large pixel sizes (in order to collect more light at the expense of resolution).

We argue here that the most likely scenario to explain the morphological and kinematical features of NGC 1427A is its passage through the hot ICM of Fornax. When a galaxy crosses the ICM of a cluster at a supersonic speed, a shock front will appear before the galaxy. This will abruptly raise the temperature and density of the ICM gas that goes through it, and so, behind the shock, the galaxy will be exposed to the action of a high thermal pressure plus the ram pressure that the shocked intracluster gas exerts upon it. Given the small sound speeds in the interstellar gas, it is very likely that another shock will form, now inside the galaxy. If the shocked interstellar gas has a cooling time[6] much shorter than the time needed by the shock wave to cross the medium, it will cool very rapidly, with the subsequent condensation that pressure equilibrium requires. In this way, dense shells of cold material follow immediately behind this '*isothermal shock*' (also called a radiative shock). Molecular clouds are formed when the column density of these cold clouds exceeds the threshold at which UV dissociation is truncated (Franco & Cox 1986), and when parts of these dense shells are fragmented and become gravitationally unstable (see Elmegreen & Elmegreen 1978) new stars are formed. This is how regions of active star formation may

---

[6]The cooling time is estimated by $t_{cool} \approx (3/2)kT/n\Lambda$, where Λ is the volume emissivity of the gas divided by the electron density and proton density (the cooling coefficient). We adopt the cooling curve of Gehrels and Williams (1993).

align around the edges of gas-rich cluster galaxies, as in the galaxies observed by Gavazzi et al. (1995).

NGC 1427A is at a projected distance of 120 kpc from NGC 1399 and moving at a relative radial velocity $V_r \approx 600$ km/s (Bureau et al. 1996), so it will be in contact with the densest parts of the ICM during $t_{ICM} \approx 2\text{x}10^8$ years, a time long enough to allow shocks propagate into the ISM and trigger new star formation. Note that, since NGC 1427A is a gas-rich galaxy, it is probably crossing the Fornax ICM for the first time. The X-ray emitting plasma in Fornax has a temperature of $1.3\text{x}10^7$ K (Rangarajan et al. 1995), and a density of $\approx 10^{-3}$ cm^{-3} at the distance of NGC 1427A (Ikebe et al. 1996). The adiabatic sound speed in a completely ionized medium with temperature T is $c_s \approx 0.15\ T^{1/2}$ km/s [7] , which for the ICM in Fornax gives $c_{ICM} \approx 500$ km/s. If we assume that this hot intracluster gas moves with NGC 1399 (around which it appears to be centered, see Fig.1 in Jones et al. 1997), then the passage of NGC 1427A across the ICM is supersonic, with an approximate Mach number $M \approx 1.2$ (a lower bound, since we only know one component of the relative velocity). A weak adiabatic shock will be leading the way of NGC 1427A through the ICM, slightly raising the temperature and density of the gas that crosses it.

The ISM in gas-rich galaxies is extremely complex, with the thermodynamic properties of the different phases varying rapidly from place to place and also in time (see, e.g., Kulkarni & Heiles 1988 for a discussion of the Milky Way's ISM; and also McKee & Ostriker 1977). We will discuss the situation for two representative states of the ISM: a hypothetical hot ionized halo, and a warm neutral hydrogen disk. In order to keep the halo in hydrostatic equilibrium in the galaxy's potential well as revealed by its rotation curve,

[7] We assume a gas with primordial abundances (90% hydrogen and 10% helium in number) so, for complete ionization the mean molecular weight is 0.59, and with just singly ionized helium it would be 0.61.

the required temperature of this hypothetical gas is $\approx 2\mathrm{x}10^5$ K. At this temperature the sound speed is $c_{halo} \approx 70$ km/s. Taking the observed mean value for the pressure of the Milky Way's ISM of $< P_{ISM} > \approx 3000$ cm^{-3}K (Kulkarni & Heiles 1988), we would have a halo density of $1.5\mathrm{x}10^{-2}$ cm^{-3}. Note that, for these conditions, the cooling time is $\approx 6\mathrm{x}10^5$ years, so constant energy input is required to keep the gas at this temperature. Assuming that most of the incident momentum from the ICM is transferred to the galaxy, we obtain $v_{ISM} \equiv v_{halo} \approx (\rho_{ICM}/\rho_{halo})^{1/2} v_{ICM} \approx 150$ km/s. Then, there would be a shock with $M \approx 2$. Applying the Rankine-Hugoniot jump conditions (Landau & Lifshitz 1979) we obtain behind this shock a temperature of $\approx 4\mathrm{x}10^5$ K and a density of $\approx 3.5\mathrm{x}10^{-2}$ cm^{-3}. With these values, the cooling time for the shocked gas in the halo would be slightly *larger* than the cooling time before the shock appeared.

For our H I phase, we may take an original temperature of 10^4 K [8]. Then the sound speed in this medium will be $c_{H\,\textsc{i}} \approx 10$ km/s (here the mean molecular weight is 1.23 if everything is neutral), and using $< P_{ISM} >$ the density would be 0.3 cm^{-3}. Again, the cooling time is short, so constant energy input is required. With these values, the velocity of the shock within the H I medium turns out to be $v_{ISM} \equiv v_{H\,\textsc{i}} \approx 30$ km/s, and now we have a shock with $M \approx 3$. Using the jump conditions we have that behind the shock the temperature of the H I is $4\mathrm{x}10^4$ K and its density 1 cm^{-3}. The cooling time of the shocked H I would be $t_{cool-H\,\textsc{i}} \approx 3000$ years, more than 20 *times shorter* than the cooling time for the unperturbed H I. The reason for this is that in the range of temperatures for the H I phase the cooling function has a positive slope, while in the range of temperatures of the

[8]This temperature is at the higher end of the observed range for this gas phase in the Galaxy, but we adopt it because at lower temperatures the cooling function is uncertain due to the varying degree of ionization. However, the conclusions will be the same as long as, below 10000 K, the slope of the cooling curve remains positive.

halo gas this slope in negative (see Fig.1 in Gehrels & Williams 1993).

The halo shock takes $\approx$ 4x10^7 years to fully cross a spherical halo with a radius of 6 kpc, while the shock in the neutral phase would need 3x10^7 years to move just 1 kpc. In both media, the cooling time is much shorter than the shock crossing time, so we could regard them as isothermal shocks. However, in the halo (where the cooling time scales before and after the shock are of the same order), this consideration does not apply if the agents that originally kept the gas at its equilibrium temperature are still present regardless of the shock, so the gas would be unable to cool. If this is not the case, all the halo gas accumulated behind the shock will cool and eventually be detected as H I. In the H I disk, the swept up gas behind the shock will surely cool rapidly, form molecular clouds, and trigger bursts of new star formation.

The rotation rate of $\approx$ 13 km/s/kpc (a lower bound, since we do not know the component of the angular velocity along the line of sight) corresponds to a rotation period of $T \approx$ 4.5x10^8 years, comparable to the crossing time, t_{ICM}, and much longer than the lifetimes of normal H II regions, $t_{H\,\textsc{ii}} \leq$ 10-15 Myr (given by the lifetimes of the very massive stars whose ionizing fluxes generated them in the first place). Thus, it is not surprising that these star forming complexes are only found along one side of the galaxy, which would have to be the side directly exposed to the shocked ICM. This explains the bow-shock appearance of the south-western edge of NGC 1427A, since the H II regions formed at the interacting side do not last long enough to reach the other side, following the rotation of the galaxy. The same scenario was proposed by de Boer et al (1998) for the interaction between the LMC and the hot Milky Way halo, giving as evidence for it the existence of a gradient in the ages of the peripheral young star clusters of the LMC in the direction expected from the relative motion between both galaxies. To obtain this kind of evidence is obviously not possible in the case of NGC 1427A because we can not resolve the young star clusters

behind the H II regions at this distance.

5. Conclusions

We have obtained the ionized gas kinematics of NGC 1427A by means of long slit spectroscopy of the brightest H II regions. The velocity field follows, on average, solid body rotation over the whole optical dimensions. Looking closer, however, there are large discrepancies in some data points, most of them associated with the diffuse component of the ionized gas in regions far away from the center of rotation.

We modeled the kinematics using two models of rotation, both assuming circular orbits in a flat disk. There is agreement between both models regarding the inclination of the axis of rotation, which is near the N-S direction. The rigid-body fit gives an angular velocity of 13 km/s/kpc, which is consistent with what is observed in this type of galaxies. The de Zeeuw and Lynden-Bell model fits the data better than the simpler solid-body but yields an unexpectedly high inclination ($\approx 80^{\circ}$) of the disk of the galaxy. Both models give large values for the merit function χ^2 because the set of velocities shows a random component that is important on small scales. This behaviour alone does not provide evidence for an interaction with the cluster environment, and may be explained by the impact that massive stars has on the ISM in Irr galaxies.

We reject the scenario in which NGC 1427A is the result of a collision with a smaller member of the cluster, because the only candidate intruder, the North Object, has a radial velocity which is nicely coincident with the general velocity pattern. However, if the inclination of the disk derived from the de Zeeuw and Lynden-Bell model is adopted, we can not place the North Object in the same disk as the rest of the H II regions. Instead, it would turn out to be a small satellite of NGC 1427A.

Several properties of NGC 1427A and its environment strongly suggest that this galaxy is interacting with the hot gas that pervades the cluster center, and we are inclined to favor this scenario. We have given quantitative estimates (although some of the numbers we used are just reasonable guesses) in order to show how the bow-shock alignment of the recent star formation in NGC 1427A is very likely due to the ram pressure from the ICM of Fornax as the galaxy crosses it. Further evidence for this scenario will have to wait for more detailed kinematics, such as interferometric Fabry-Perot imaging and good resolution stellar spectra. Then it will be possible to compare the kinematics of the gas component with that of the stars, which may be very different in the ram pressure scenario. Also, high resolution mapping in H I should show signs of this interaction, such as stripped gas and sudden truncation and asymmetries in the distribution of the neutral gas, as observed in the Virgo Cluster (Cayatte et al. 1990) and even in groups of galaxies (Davis et al. 1997).

Acknowledgements We thank Bill Kunkel for allowing us to use part of his observing time, and without him this work wouldn't have started. We also thank Guillermo Tenorio-Tagle for invaluable discussions and insights; María Teresa Ruiz and Michael Hilker for their interest and help in the continuation of this work; and Roberto Terlevich for useful comments. We thank to Fondecyt Chile for support through "Proyecto FONDECyT 8970009".

REFERENCES

Barnes, J., & Hernquist, L. 1991, ApJ, 370, L65

Bomans, D.J., Chu, Y.-H., & Hopp, U. 1997, AJ, 113, 1678

Bureau, M., Mould, J. R., & Staveley-Smith, L. 1996, ApJ, 463, 60

Butcher, H., & Oemler, A., Jr. 1978, ApJ, 219, 18

Byrd, G., & Valtonen, M. 1990, ApJ, 350, 89

Cayatte, V., van Gorkom, J. H., Balkowski, & C., Kotanyi, C. 1990, AJ, 100, 604

Cellone, S. A., & Forte, J. C. 1997, AJ, 113, 1239

Dahlem, M., Dettmar, R.-J., & Hummel, E. 1994, A&A, 290, 384

Davis, D., Keel, W., Mulchaey, J., & Henning, P. 1997, AJ, 114, 613

de Boer, K. S., Braun, J. M., Vallenari, A., & Mebold, U. 1998, A&A, 329, L49

Della Valle, M., Kissler-Patig, M., Danziger, J., & Storm, J. 1998, MNRAS, 299, 267

de Zeeuw, P. T., & Lynden-Bell, D. 1988, MNRAS, 232, 419

de Vaucouleurs, G., de Vaucouleurs, A., Corwin, H. G., Buta, R. J., Paturel, G., & Fouqué, P. 1991, Third Reference Catalogue of Bright Galaxies

Elmegreen, B. G., & Elmegreen, D. M. 1978, ApJ, 220, 1051

Evrard, A.E. 1991, MNRAS, 248, Short Communications 8p-10p

Ferguson, H. C., & Sandage, A. 1988, AJ, 96, 1520

Franco, J., & Cox, D. P. 1986, PASP, 98, 1076

Gallagher, J., & Hunter, D. 1984, Ann. Rev. Astron. Astroph. 22, 37

Gavazzi, G., Contursi, A., Carrasco, L., Boselli, A., Kennicutt, R., Scodeggio, M., & Jaffe, W. 1995, A&A, 304, 325

Gehrels, N., & Williams, E. D. 1993, ApJ, 418, L25

Giovanelli, R., & Haynes, M. 1985, ApJ, 292, 404

Gratton, R. G., Fusi Pecci, F., Carretta, E., Clementini, G., Corsi, C. E., & Lattanzi, M. G. 1997, in Hipparcos Venice'97 Symposium (ESA SP-402)

Gregg, M. D., & West, M. J. 1998, Nature, 396, 549

Grillmair, C., Forbes, D., Brodie, J., & Elson, R. 1999, AJ, 117, 167

Gunn, J., & Gott, J. R. 1972, ApJ, 176, 1

Gunn, J. 1989, in The Epoch of Galaxy Formation, eds. Frenk, C. S. et al. (Kluwer, Dordretch), 167

Henriksen, M. J., & Byrd, G. 1996, ApJ, 459, 82

Hilker, M., Bomans, D. J., Infante, L., & Kissler-Patig, M. 1997, A&A, 327, 562

Hilker, M. 1998, PhD. Thesis, University of Bonn

Huchtmeier, W. K., & Richter, O. -G. 1988, A&A, 203, 237

Hunter, D., & Gallagher, J. 1986, PASP, 98, 5

Hunter, D., & Gallagher, J. 1997, ApJ, 475, 65

Ikebe, Y., Ezawa, H., Fukuzawa, Y., Hirayama, M., Ishisaki, Y., Kikuchi, K., Kubo, H., Makishima, K., Matsushita, K., Ohashi, T., Takabashi, T., & Tamura, T. 1996, Nature, 379, 427

Jensen, J., Tonry, J., & Luppino, G. 1998, ApJ, 505, 111

Jones, C., Stern, C., Forman, W., Breen, J., David, L., Tucker, W., & Franx, M. 1997, ApJ, 482, 143

Kohle, S., Kissler-Patig, M., Hilker, M., Richtler, T., Infante, L., & Quintana, H. 1996, A&A, 309, L39

Kulkarni, S. R., & Heiles, C. 1988, in Galactic and Extragalactic Radio Astronomy, ed. G. L. Verschuur & K. I. Kellermann (Springer-Verlag), 95

Kunkel, W. E., Demers, S., Irwin, M. J., & Albert, L. 1997, ApJ, 488, L129

Landau, L. D., & Lifshitz, E. M. 1979, in Fluid Mechanics (Pergamon Press), 331

Lee, M. G., Kim, E., & Geisler, D. 1997, AJ, 114, 1824

Lynds, R., & Toomre, A. 1976, ApJ, 209, 382

Martin, C. 1997, ApJ, 491, 561

Martin, C. 1998, ApJ, 506, 222

McKee, C. F., & Ostriker, J. P. 1977, ApJ, 218, 148

Moore, B., Katz, N., Lake, G., Dressler, A., & Oemler, A. 1996, Nature, 379, 613

Patterson, R., & Thuan, T. X. 1992, ApJ, 400, L58

Phookun, B., & Mundy, L. G. 1995, ApJ, 453, 154

Press, W. H., Teukolsky, S. A., Vetterling, W. T., & Flannery, B. P. 1992, in Numerical Recipes (Cambridge University Press)

Rangarajan, F. V. N., Fabian, A. C., Forman, W. R., & Jones, C. 1995, MNRAS, 272, 665

Richtler, T., Grebel, E. K., Domgörgen, H., Hilker, M., & Kissler-Patig, M. 1992, A&A, 264, 25

Roberts, M. 1975, in Galaxies and the Universe, ed. A. Sandage, M. Sandage, & J. Kristian (Chicago Press), 326

Roberts, M. S., & Haynes, M. P. 1994, Ann. Rev. Astron. Astroph. 32, 115

Theys, J. C., & Spiegel, E. A. 1977, ApJ, 212, 616

This manuscript was prepared with the AAS LaTeX macros v4.0.

Table 1. The data.

label	x (pix)	y (pix)	v_{helio} (km/s)	Δv (km/s)	
1	343.2	441.13	1955.1	10.2	
2	238.8	441.13	2034.2	5.26	
3	209.8	441.13	2042.6	3.62	
4	161.8	441.13	2038.6	5.66	
5	143.6	441.13	2047.9	9.32	
6	348.6	432.56	1983.9	5.07	
7	237.2	432.56	2019.7	5.47	
8	215.6	432.56	2041.4	5.06	
9	146.4	432.56	2054.1	3.65	
10	231.9	423.96	2018.1	4.21	
11	167.4	423.96	2046.8	4.36	
12	147.0	423.96	2076.3	3.74	
13	343.3	415.36	1984.2	4.98	
14	236.2	415.36	2019.9	5.09	
15	189.2	415.36	2030.9	8.40	
16	151.3	415.36	2058.1	5.12	
17	119.4	415.36	2086.9	5.12	
18	88.9	415.36	2060.9	9.45	
19	231.2	421.73	2016.2	3.79	
20	205.7	396.20	2035.9	4.49	
21	185.2	377.20	2056.3	9.49	
22	173.7	366.20	2053.4	9.59	
23	164.7	353.70	2032.3	9.69	
24	125.4	319.89	2035.4	11.3	
25	257.2	249.90	2033.4	4.00	(N.O.)
26	247.7	243.70	2024.3	9.00	(N.O.)
27	163.6	324.70	2045.8	3.63	
28	127.0	362.10	2068.0	9.26	

Table 1—Continued

label	x (pix)	y (pix)	v_{helio} (km/s)	Δv (km/s)
29	111.3	379.50	2108.4	7.72

[a]N.O. = North Object

Fig. 1.— Isophotal contours of a B-band image of NGC 1427A (Hilker et al. 1997) with the slit positions superimposed. The North Object (N.O.) is indicated with a circle. The isophotal levels were chosen in order to enhance the contrast between the H II regions and the main stellar body. The object at approximate coordinates (60,280) is a background galaxy.

Fig. 2.— Sample spectra of H II regions in NGC 1427A at different signal-to-noise ratios (S/N) for the Hα line. Units of the vertical axis are CCD counts.

Fig. 3.— Error analysis. (a) The uncertainty in the center of the Hα line as a function of the signal-to-noise ratio. An error of 0.1 $\AA$ translates to 4.5 km/s in velocity. (b) The distribution of residuals in the method of error estimation using night skylines. The solid curve is a Gaussian fit to the points. It is centered at 0.04 $\AA$ and has a standard deviation of 0.18 $\AA$.

Fig. 4.— The radial velocities of the H II regions in NGC 1427A vs. the distance to the axis of rotation found with the solid-body model (6° counter-clockwise from the N-S direction). Note the agreement between the velocities of points in the North Object (N.O.) with the overall rotation of the galaxy. Filled circles represent the peaks of the Hα emission, and blank circles the diffuse emission at some distance from the bright H II regions.

Fig. 5.— V image of NGC 1427A (Hilker et al. 1997), showing the alignment of H II regions along half of its perimeter. The positions of the axis of rotation and the center of rotation found with the de Zeeuw & Lynden-Bell model are shown, as well as the direction to the giant ellipticals at the cluster center.

Fig. 6.— Circular velocities on the plane of the disk of NGC 1427A, according to the best-fit model of de Zeeuw & Lynden-Bell. The triangles represent points very close to the axis of rotation. The two points located at the North Object also are triangles, but they are not shown because they would fall at ≈ 30 kpc. Filled symbols are the peaks of the Hα emission,

and blank symbols the diffuse emission. Also shown are the rotation curves with the values of p between which the data can not distinguish.

Fig. 7.— Detail of the V image of NGC 1427A, showing possible large scale expanding shells in the interstellar medium. The arrows mark structures with diameters of 0.7 and 1.1 kpc.

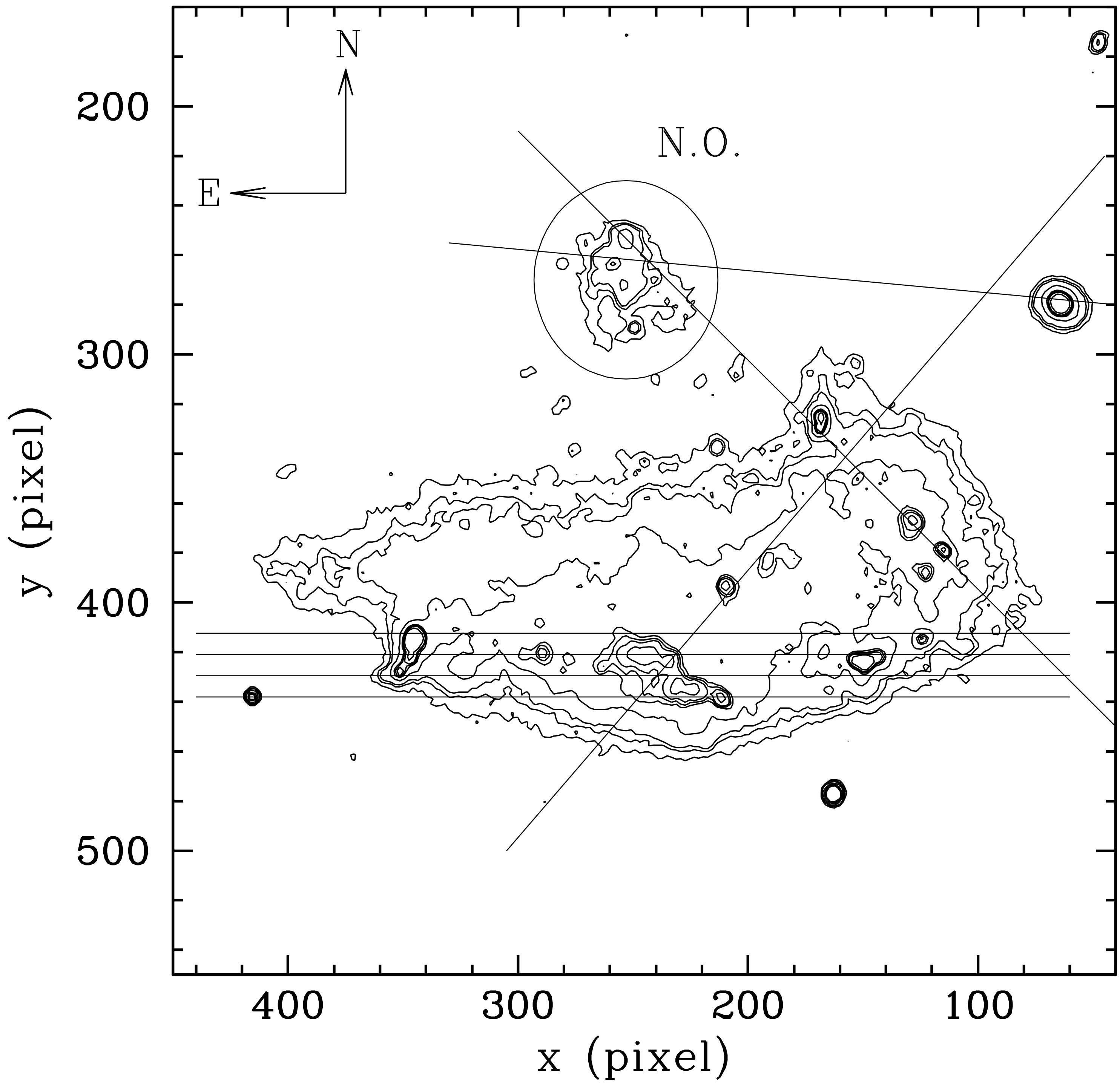
N
E
N.O.
200
300
400
500
y (pixel)
400
300
200
100
x (pixel)

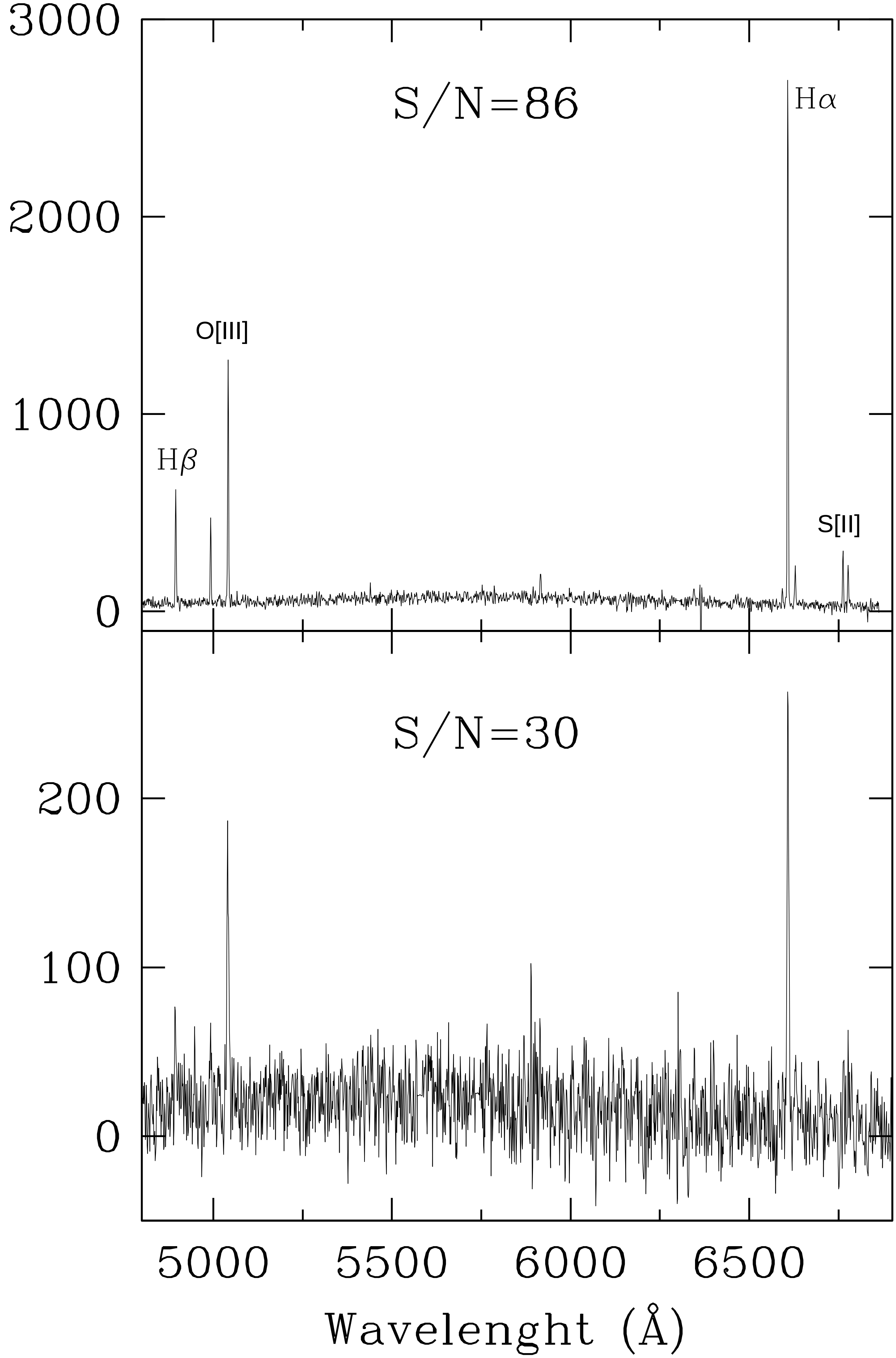

3000
2000
1000
0
S/N=86
Hα
O[III]
Hβ
S[II]
S/N=30
200
100
0
5000
5500
6000
6500
Wavelenght (Å)

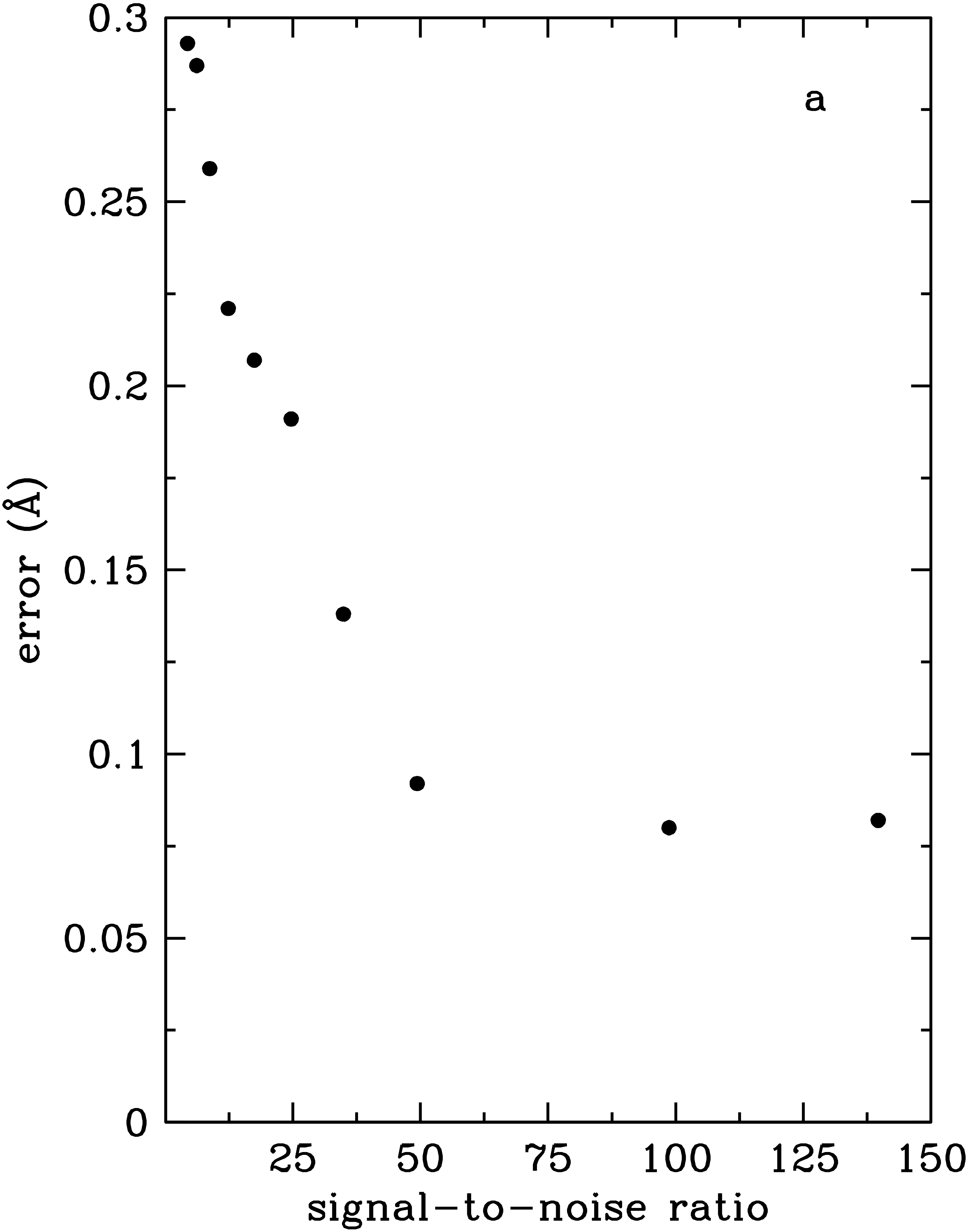

a
error (Å)
0
0.05
0.1
0.15
0.2
0.25
0.3
25
50
75
100
125
150
signal-to-noise ratio

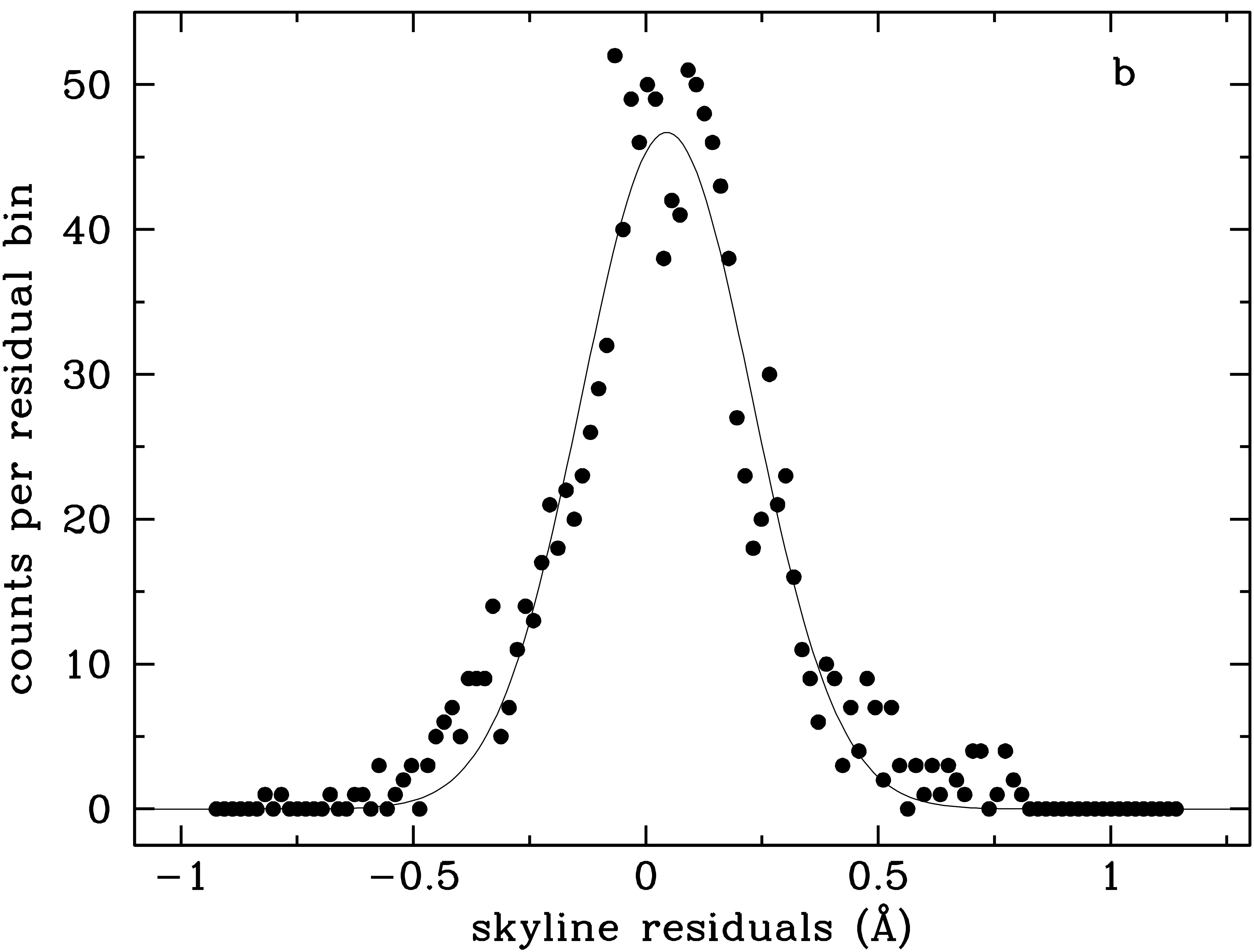
b
counts per residual bin
0
10
20
30
40
50
−1
−0.5
0
0.5
1
skyline residuals (Å)

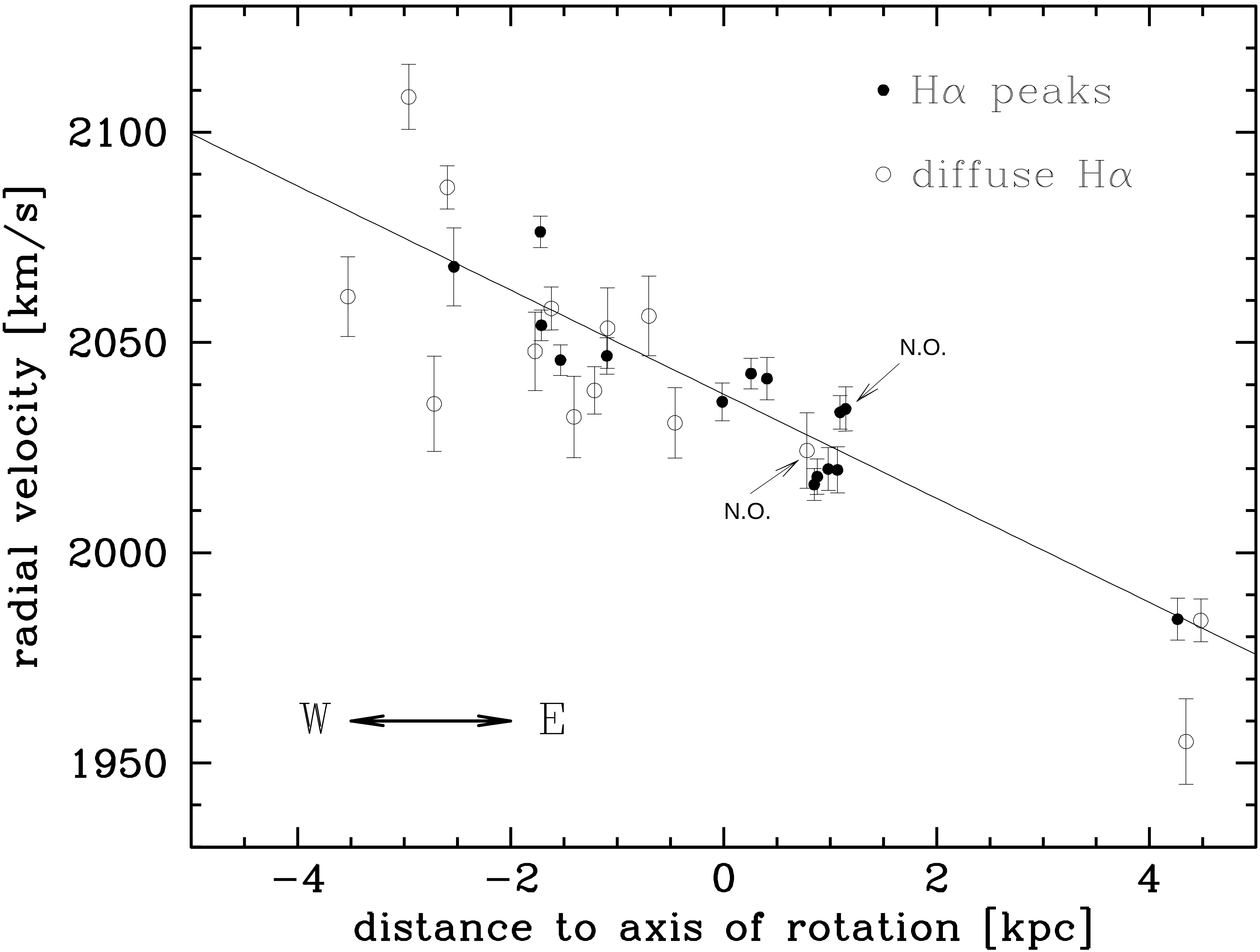

Hα peaks
diffuse Hα
N.O.
N.O.
W
E
2100
2050
2000
1950
radial velocity [km/s]
−4
−2
0
2
4
distance to axis of rotation [kpc]

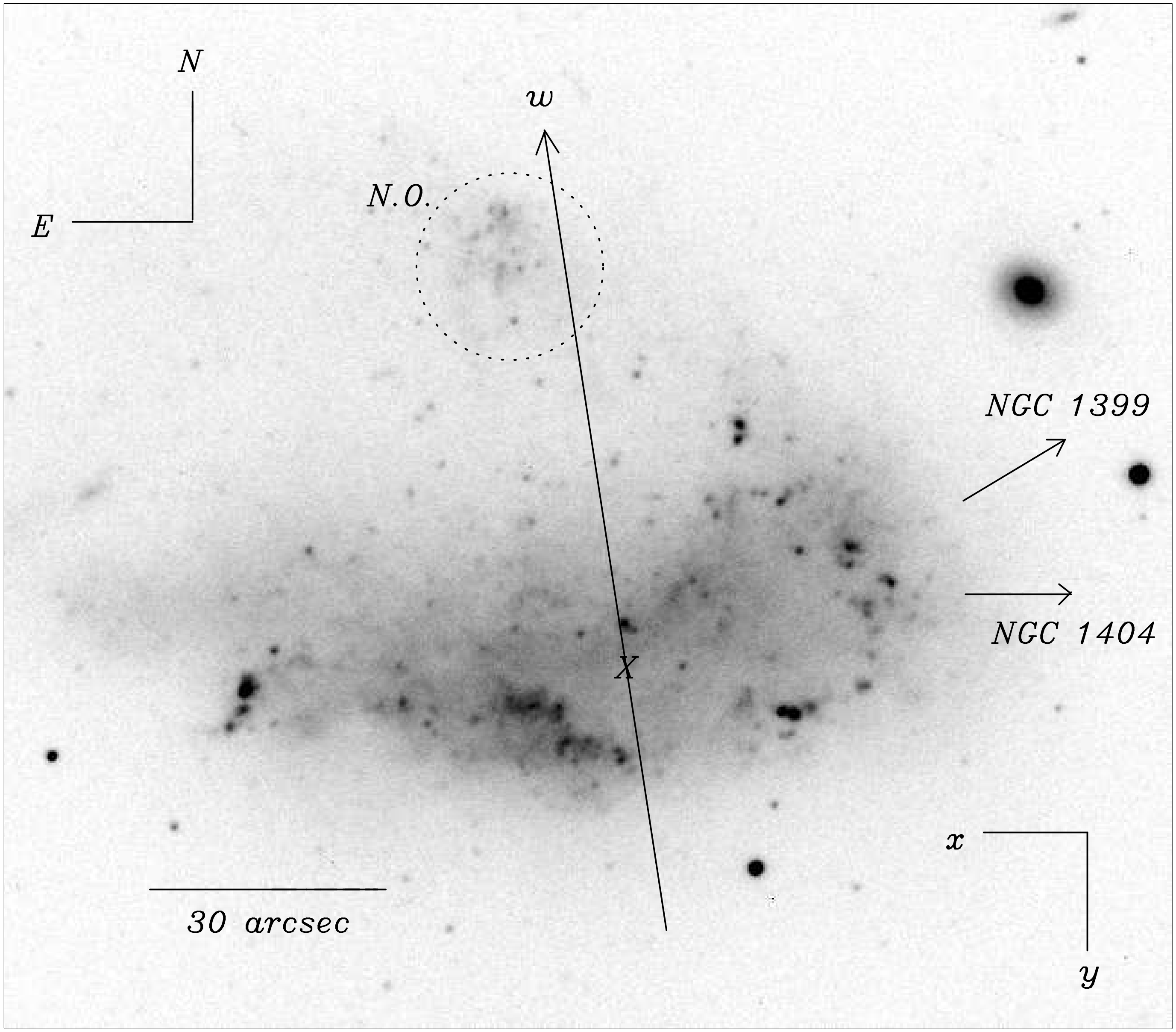
N
E
w
N.O.
NGC 1399
NGC 1404
X
x
y
30 arcsec

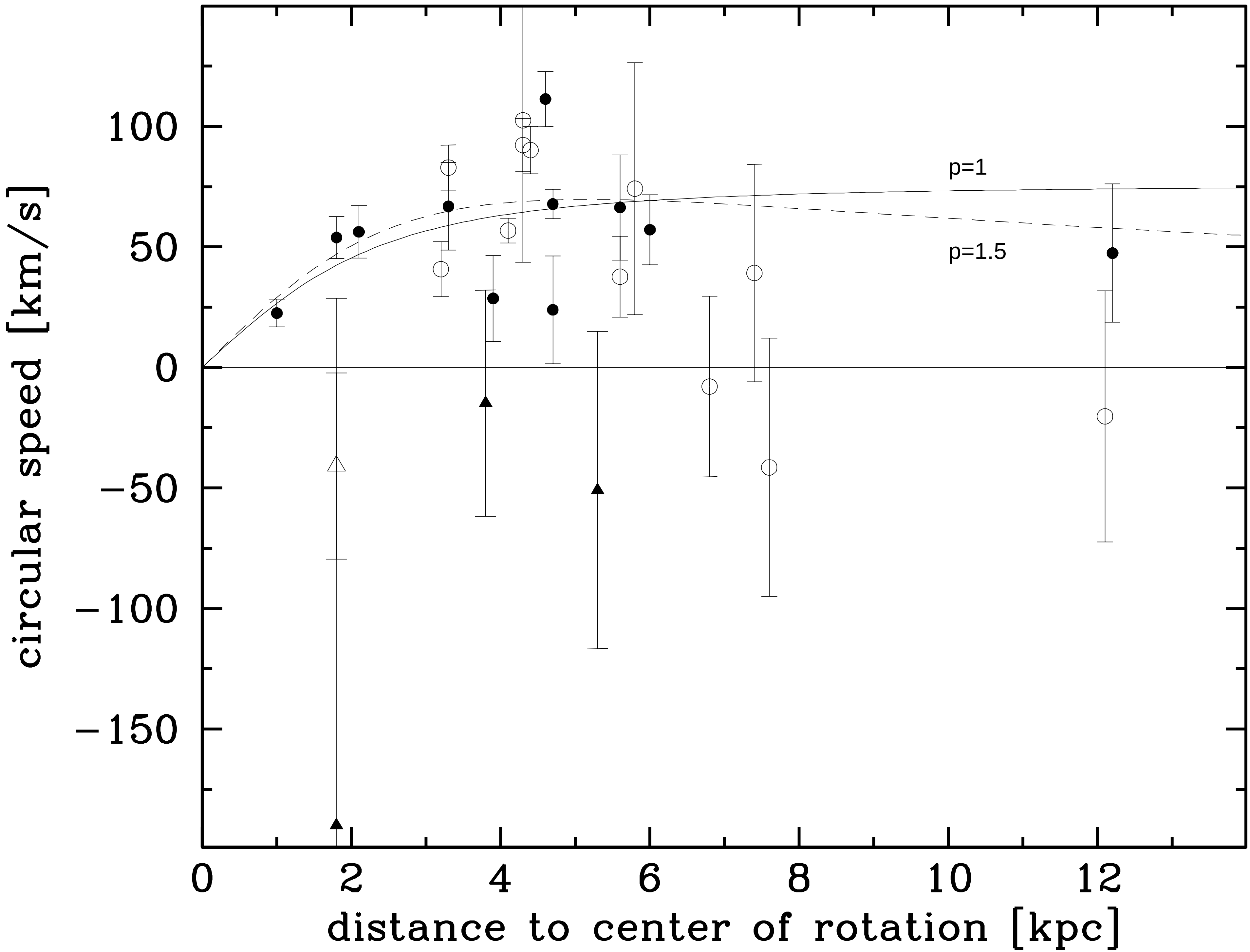

circular speed [km/s]
100
50
0
−50
−100
−150
p=1
p=1.5
0
2
4
6
8
10
12
distance to center of rotation [kpc]

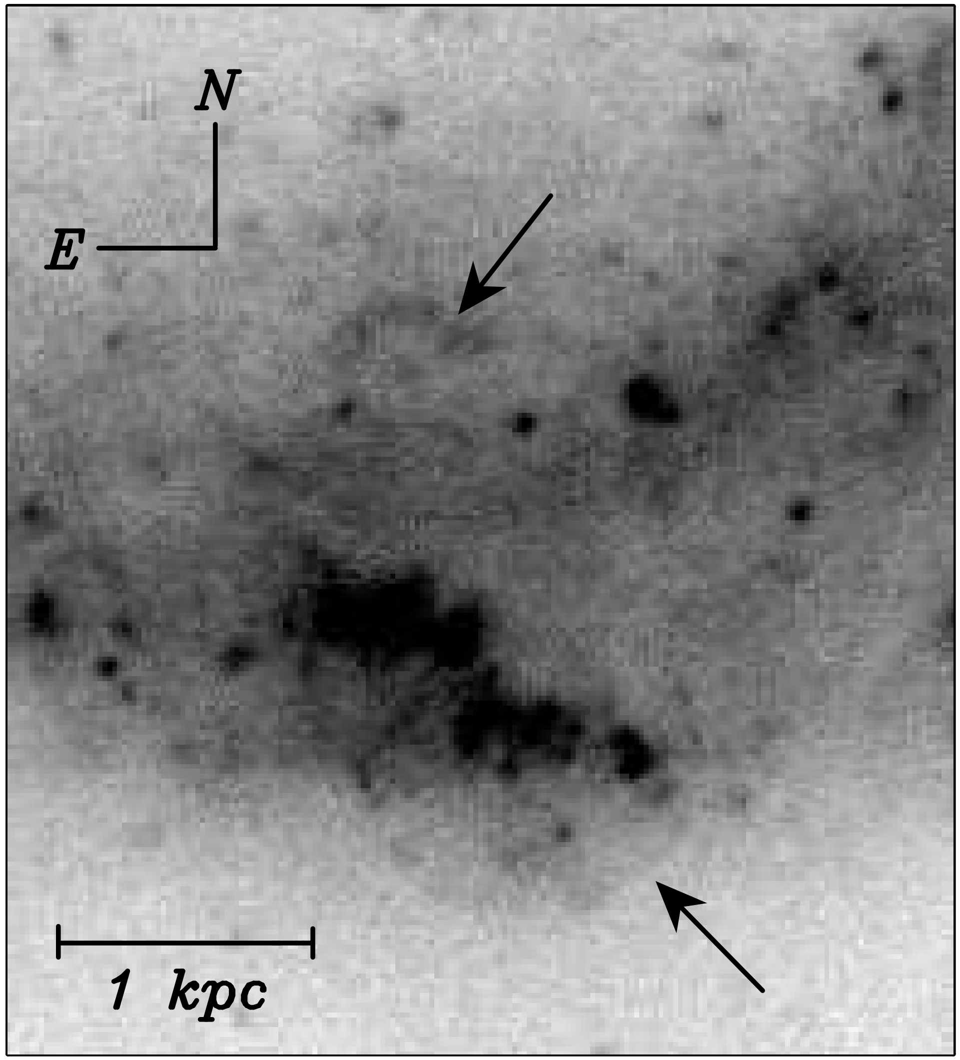
N
E
1 kpc